JOC The Journal of Organic Chemistry

Article

pubs.acs.org/joc

Mandelalides A−D, Cytotoxic Macrolides from a New *Lissoclinum* Species of South African Tunicate

Justyna Sikorska,[†] Andrew M. Hau,[†] Clemens Anklin,[‡] Shirley Parker-Nance,[§] Michael T. Davies-Coleman,[∥] Jane E. Ishmael,[†] and Kerry L. McPhail*[,†]

[†]Department of Pharmaceutical Sciences, College of Pharmacy, 203 Pharmacy Building, Oregon State University, Corvallis, Oregon 97331, United States

[‡]Bruker BioSpin, 15 Fortune Drive, Billerica, Massachusetts 01821, United States

[§]Department of Zoology, Nelson Mandela Metropolitan University, PO Box 77000, Port Elizabeth 6031, South Africa

[∥]Department of Chemistry, Rhodes University, PO Box 94, Grahamstown 6140, South Africa

Supporting Information

ABSTRACT: Mandelalides A−D are variously glycosylated, unusual polyketide macrolides isolated from a new species of *Lissoclinum* ascidian collected from South Africa, Algoa Bay near Port Elizabeth and the surrounding Nelson Mandela Metropole. Their planar structures were elucidated on submilligram samples by comprehensive analysis of 1D and 2D NMR data, supported by mass spectrometry. The assignment of relative configuration was accomplished by consideration of homonuclear and heteronuclear coupling constants in tandem with ROESY data. The absolute configuration was assigned for mandelalide A after chiral GC-MS analysis of the hydrolyzed monosaccharide (2-*O*-methyl-α-L-rhamnose) and consideration of ROESY correlations between the monosaccharide and aglycone in the intact natural product. The resultant absolute configuration of the mandelalide A macrolide was extrapolated to propose the absolute configurations of mandelalides B−D. Remarkably, mandelalide B contained the C-4′ epimeric 2-*O*-methyl-6-dehydro-α-L-talose. Mandelalides A and B showed potent cytotoxicity to human NCI-H460 lung cancer cells (IC_{50}, 12 and 44 nM, respectively) and mouse Neuro-2A neuroblastoma cells (IC_{50}, 29 and 84 nM, respectively).

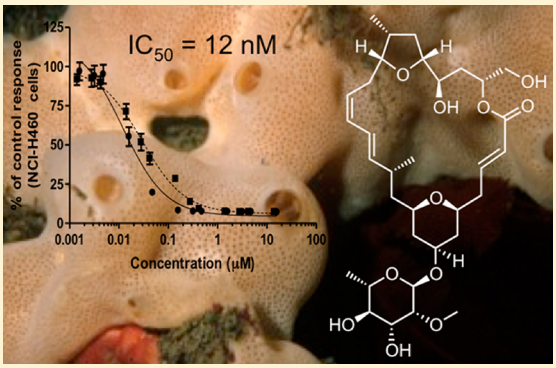

INTRODUCTION

Over the last 50 years, ascidians have been shown to be a prolific source of natural products with promising biomedical potential.[1] Indeed, ascidian-derived natural products have yielded promising drug leads, among which ecteinascidin 743 (Yondelis) and dehydrodidemnin B (Aplidin) are in clinical use for the treatment of specific cancers.[2] The diverse chemotypes reported from *Lissoclinum* species collected globally have important biological properties that range from cancer cell toxicity to antifungal and antibacterial activities,[1] and include peptides, alkaloids, chlorinated diterpenes, polyether amides, lactones, and macrolides such as haterumalide B[3] and patellazoles B and C.[4,5] It has been noted that many secondary metabolites isolated from *Lissoclinum*, as well as other ascidians species, are present in bacteria, sponges, and mollusks.[6−8] This diversity of ascidian metabolites can be explained by the fact that tunicates are often hosts to cyanobacterial and heterotrophic bacterial symbionts, as well as being fed upon by predatory mollusks.[7−10] Therefore, identification of the biogenetic origin of ascidian natural products is very often challenging.[11] This is highlighted by the recent isolation of didemnin B (an analog of Aplidin) from the α-proteobacterium *Tistrella mobiliz*.[8,12] This compound was originally identified from the ascidian *Aplidium albicans* and is biosynthetically similar to peptides from the marine cyanobacterium *Lyngbya majuscula*[8] (now *Moorea producta*).

In our search for new potential anticancer compounds, we encountered the highly cytotoxic organic extract (IC_{50} = 0.7 μg/mL in NCI-H460 lung cancer cells) of a new *Lissoclinum* species from Algoa Bay, South Africa. Bioassay-guided fractionation of this extract, yielded a series of new macrolides, named mandelalides A−D (**1**−**4**), two of which were tested and show good cytotoxicity to mouse Neuro-2A neuroblastoma and human NCI-H460 lung cancer cells. While the relative configuration of the compounds could be assigned from analysis of ROESY data in tandem with homonuclear ($^3J_{HH}$) and heteronuclear ($^{2,3}J_{CH}$) coupling constants, the assignment of absolute configuration relied on hydrolysis of the glycosylated mandelalide A and chiral GC-MS analysis of the released monosaccharide. Remarkably, mandelalide A contains 2-*O*-methyl-α-L-rhamnose, while mandelalide B contains the C-4′ epimer 2-*O*-methyl-6-dehydro-α-L-talose.

Received: April 29, 2012
Published: June 19, 2012

   dx.doi.org/10.1021/jo3008622 | J. Org. Chem. 2012, 77, 6066−6075

RESULTS AND DISCUSSION

A new *Lissoclinum* ascidian species was collected from White Sands Reef in Algoa Bay, South Africa. The organic extract (1.45 g) was subjected to bioassay-guided fractionation through consecutive LH-20 and RP-HPLC chromatography to yield mandelalides A–D (**1**–**4**), of which mandelalide D degraded to deacylmandelalide D (**4b**).

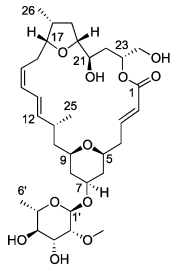

1

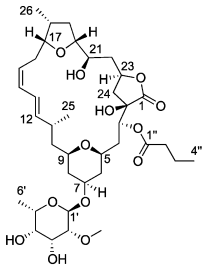

2

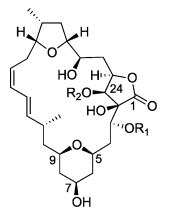

3 R_1 = $COCH_2CH_2CH_3$, R_2 = OH
4 R_1 = $COCH_2CH_2CH_3$, R_2 = $COCH_2CH_2CH_3$
4b R_1 = H, R_2 = H

The HR-ESI-MS data for mandelalide A (**1**) gave a pseudomolecular ion $[M + Na]^+$ at m/z 647.3394, which is consistent with a molecular formula of $C_{33}H_{52}O_{11}$, and implies 8 degrees of unsaturation. The ^{13}C and multiplicity-edited HSQC NMR spectra for compound **1** (Table 1) indicated the presence of an ester carbonyl (δ_C 167.4), fourteen sp^3 methines, twelve of which were oxygen-bearing (δ_C 94.2–68.1, 37.3 and 34.2), six olefinic methines (δ_C 147.1, 141.5, 131.3, 126.9, 123.9 and 123.1), eight methylenes (δ_C 66.1, 43.1, 39.7, 38.8, 37.6, 36.8, 34.1 and 31.1) and four methyl groups (δ_C 59.1, 18.3, 17.7 and 14.5). Interpretation of COSY and TOCSY correlations delineated two spin systems, one comprising 25 carbons from C-2 to C-26 (Figure 1a, fragment A), and the other of 6 carbons from C-1′ to C-6′ (Figure 1a, fragment B). The acquisition of a semiphase sensitive HMBC[13] optimized for a 4 Hz coupling constant (Figure S6, Supporting Information), revealed a correlation between δ_H 5.23 (H-23) and δ_C 167.4 (C-1) that indicated cyclization of fragment A into a 23-carbon macrolactone. The C-1 carbonyl also showed HMBC correlations from the olefinic H-2 and H-3 multiplets, for which a $^3J_{HH}$ of 15.5 Hz indicated an *E* double bond geometry. An HMBC correlation between H-9 (δ 3.32) and C-5 (δ 73.9) delineated a tetrahydropyran ring, while a correlation between H-17 (δ 3.98) and C-20 (δ 83.2) was consistent with a tetrahydrofuran ring, both within fragment A (Table 1, Figure 1a). The four contiguous (TOCSY-coupled) olefinic methines CH-12 to CH-15 (δ_H 5.45, 6.28, 6.05, and 5.28 ppm) were consistent with a conjugated diene, situated β to the tetrahydrofuran and γ to the tetrahydropyran on the basis of HMBC correlations from H-15 to C-17 and H-12 to C-10, respectively. From homonuclear coupling constant values ($^3J_{HH}$ = 14.8 and 10.8 Hz, respectively) it was evident that the geometry of H-12 and H-13 is *trans*, while H-14 and H-15 are *cis*. Knowing that $^3J_{HH}$ values are not sufficiently characteristic to assign the orientation between H-13 and H-14, ROESY data were examined.[14] ROEs between H-12 and H-10a, as well as between H-13 and H-16b, suggested an *anti* orientation for H-13 and H-14 (Figure 1b). In the case of fragment B, the downfield shift of C-1′ (δ_C 94.2), the presence of four midfield oxymethine ^{13}C resonances, an upfield methyl doublet (CH_3-6′, δ_C 17.7, δ_H 1.27) and an HMBC correlation between H-1′ (δ 5.02) and C-5′ (δ 68.1) suggested that fragment B is a 6-dehydro monosaccharide. An HMBC correlation between H-2′ (δ 3.40) and deshielded methyl C-7′ (δ 59.1) indicated methylation of the C-2′ hydroxyl group. An HMBC correlation from H-7 (δ 3.82) to C-1′ placed the monosaccharide (fragment B) at C-7 of fragment A.

The second compound characterized, mandelalide B (**2**), was assigned a molecular formula of $C_{37}H_{58}O_{13}$, based on HR-ESI-MS data for $[M + Na]^+$ m/z 733.3773, which is consistent with 9 degrees of unsaturation. Inspection of the ^1H and ^{13}C NMR spectra for mandelalide B (**2**) suggested that it was structurally related to mandelalide A (**1**). However, the ^1H NMR spectrum for **2** lacked the coupled olefinic signals at δ 6.01 (H-2) and 6.97 (H-3) and the relatively deshielded diastereotopic H_2-24 signals at δ 3.81 and 3.61. Instead an additional oxymethine double doublet at δ 5.48 was evident, as well as a methyl triplet (δ_H 0.95) indicative of an aliphatic chain. Correspondingly, comparison of the ^{13}C NMR spectra for **1** and **2** revealed the absence of olefinic ^{13}C resonances at δ 123.1 (C-2) and 147.1 (C-3) from the spectrum for **2**, and the presence of two additional midfield ^{13}C resonances (δ 79.3 and 69.5), as well as a second carbonyl resonance (δ_C 173.6). These data accounted for 8 of the 9 degrees of unsaturation, implying the presence of an additional cycle in **2**. The analysis of HSQC and HMBC data for **2** permitted assignment of an oxygenated quaternary C-2 (δ 79.3) and an oxymethine CH-3 (δ 69.5, δ 5.48). While the same C-1/C-23 macrolactone linkage was apparent in both compounds, two-and three-bond HMBC correlations from H_2-24 (δ 1.93, 2.39) to C-2 and C-3, respectively, indicated a C-2/C-24 bond in **2**. These data described a γ-butyrolactone ring around the ester linkage of the mandelalide B macrocycle. Placement of the second carbonyl carbon (δ_C 173.6) in a butyrate substituent at C-3 was facilitated by HMBC correlations to δ_C 173.6 from δ_H 5.48 (H-3), as well as 2.35 (H_2-2″) and 1.67 (H_2-3″). Further analysis of NMR data confirmed the presence of a 2-*O*-methyl-6-dehydro sugar in **2**. However, differences in both ^1H and ^{13}C shifts for CH-3′ to CH-6′ compared to compound **1** suggested a different relative configuration for the monosaccharide in **2** (Table 2).

The HR-ESI-MS data ($[M + Na]^+$ m/z 589.2970) for mandelalide C (**3**) supported a molecular formula of $C_{30}H_{46}O_{10}$, for 8 degrees of unsaturation. The ^1H NMR spectrum for **3** was reminiscent of that for **2**. However, a careful comparison of the two spectra revealed the absence of midfield glycosidic signals in the ^1H spectrum for **3**. Similarly, inspection of the ^{13}C NMR spectrum for **3** showed a lack of midfield resonances for a methoxy methyl (δ 59.6, C-7′ in **2**), anomeric carbon (δ 94.8, C-1′ in **2**), and other glycosidic carbons. Together, the MS and 1D NMR data for compound **3** indicated that the structure of **3** is related to the aglycone of mandelalide B (**2**, Table 2). Indeed, the only difference between the ^{13}C NMR signals for the aglycones of compounds **2** and **3** was a relatively downfield methine resonance at δ 72.2 in the spectrum for **3**, compared to the methylene signal at δ 37.9 (C-24) in the spectrum for **2**. This methine was HSQC-correlated to a 1H doublet at δ_H 3.98, and could be assigned to an oxymethine CH-24 on the basis of HMBC correlations from the latter ^1H doublet to C-1, C-2, C-3 and C-23. Thus, considering its MS and NMR data, mandelalide C (**3**) could be assigned as the C-24 hydroxylated aglycone of mandelalide B (**2**). Unfortunately, an attempt to crystallize mandelalide C (0.5 mg) was unsuccessful and degradation of the compound over several months prevented the acquisition of additional spectroscopic or biological data.

dx.doi.org/10.1021/jo3008622 | J. Org. Chem. 2012, 77, 6066–6075

Table 1. NMR Data for Mandelalide A (1) in $CDCl_3$

no.	δ_C (mult)	δ_H (J in Hz)	COSY	HMBC[a]	TOCSY	ROESY
1	167.4 (s)					
2	123.1 (d)	6.01 (dd, 15.5, 1.2)	3, 4a	1, 4	3, 4a, 4b, 5, 6ax, 6eq	3[b], 4a, 4b, 5
3	147.1 (d)	6.97 (ddd, 15.2, 10.4, 4.6)	2, 4a, 4b	1, 2, 4, 5	2, 4a, 4b, 5, 6ax, 6eq	3[b], 4a[b], 4b[b], 5
4a	38.8 (t)	2.36 (m)	2, 3	2, 3, 5, 6	2, 3, 5, 6ax, 6eq, 7	2, 3[b], 5[b], 6ax[b], 6eq
4b		2.39 (ddd, 14.1, 10.6, 10.6)	3, 5	2, 3, 5, 6	2, 3, 5, 6ax, 6eq, 7	2, 3[b], 5[b], 6ax[b], 6eq
5	73.9 (d)	3.36 (dddd, 11.4, 11.4, 2.3, 2.3)	4a, 4b, 6ax, 6eq	3, 4	2, 3, 4a, 4b, 6ax, 6eq, 7, 8ax, 8eq	2, 3, 4a, 4b, 6eq, 7
6ax	37.6 (t)	1.20 (m)	5, 6eq, 7	4, 5, 8	3, 4a, 4b, 5, 6eq, 7	4b[b], 7
6eq		2.02 (dddd, 12.6, 4.4, 2.3, 1.6)[c]	5, 6ax, 7, 8eq	7, 8	4a, 4b, 5, 6ax, 7, 8ax,	6ax[b], 4a, 4b, 5, 7, 1′
7	73.1 (d)	3.82 (dddd, 11.1, 10.5, 4.4, 4.4)[c]	6ax, 6eq, 8ax, 8eq	8, 9, 1′	4a, 4b, 5, 6ax, 6eq, 8ax, 8eq, 9	5, 6ax[b], 6eq, 8ax[b], 8eq, 9, 1′
8ax	39.7 (t)	1.22 (m)	7, 8eq, 9	6, 7, 9, 10	6eq, 7, 8eq, 9, 10b	6eq[b], 7, 8eq[b]
8eq		1.87 (m)	6eq, 7, 8ax, 9	6, 7	6eq, 7, 8ax, 9, 10a, 10b	7, 8ax[b], 9, 10b, 5′
9	72.5 (d)	3.32 (dddd, 11.2, 11.2. 2.2, 2.2)[c]	8ax, 8eq, 10a, 10b	5, 7	6eq, 7, 8ax, 8eq, 10a, 10b, 11, 12, 13, 25	7, 8eq, 10a, 10b[b], 25
10a	43.1 (t)	1.21 (ddd, 15.2, 9.6, 2.2)[c]	9, 10b, 11	11, 12, 25	8eq, 9, 10b, 12, 13, 14, 25	8eq, 9, 10b[b], 11[b], 12, 25
10b		1.51 (ddd, 15.2, 11.2, 3.7)[c]	9, 10a, 11	8, 9, 11, 12, 25	8ax, 8eq, 9, 10a, 11, 12, 13, 25	8eq, 9[b], 10a[b], 11, 25
11	34.2 (d)	2.37 (dqd, 9.6, 6.5, 3.7)[c]	10a, 10b, 12, 25	10, 12, 25	8ax, 8eq, 9, 10a, 10b, 11, 12, 13, 14, 15	10a[b], 10b, 12[b], 13, 25[b]
12	141.5 (d)	5.45 (dd, 14.8, 9.7)	11, 13	10, 11, 14, 25	9, 10a, 10b, 11, 13, 14, 15, 16a, 16b, 25	11[b], 10a, 13[b], 14[b], 25
13	123.9 (d)	6.28 (dd, 14.8, 11.0)	12, 14	10, 11, 14, 15	10a, 10b, 11,12, 14, 15, 16a, 16b, 17, 25	11, 12[b], 14[b], 15[b], 16b, 21
14	131.3 (d)	6.05 (dd, 10.9, 10.9)	13, 15	12, 13,16, 17	10a, 11, 12, 13, 15, 16a, 16b, 17, 25	12[b], 13[b], 15[b], 16a
15	126.9 (d)	5.28 (ddd, 10.8, 10.8, 5.6)	14, 16a, 16b	13, 16, 17	12, 13, 14, 16a, 16b, 17, 18, 26	13[b], 14[b], 16a, 16b[b], 17[b]
16a	31.1 (t)	1.88 (m)	14, 15, 16b, 17	14, 15, 17	12, 13, 14, 15, 16b, 17, 18, 19a, 26	14, 15, 16b, 17[b], 26
16b		2.28 (ddd, 13.1, 11.4, 11.4)	15, 16a, 17	14, 15, 17, 18	12, 13, 14, 15, 16a, 17, 18, 19a, 19b, 26	13,15[b],16a,17[b],19a,21,26
17	81.0 (d)	3.98 (ddd, 11.1, 8.1, 1.8)	16a, 16b, 18	15, 19, 20	14, 15,16a, 16b, 18, 19a, 19b, 20, 21, 26	15, 16a[b], 16b[b],18, 26
18	37.3 (d)	2.52 (dddq, 12.0, 7.0, 7.0, 7.0)[c]	17, 19a, 19b, 26	16, 17, 19, 26	15, 16a, 16b,17, 19a, 19b, 20,21, 22a, 26	17, 19a[b], 19b, 20, 26[b]
19a	36.8 (t)	1.17 (ddd, 11.9, 11.9, 10.3)	18, 19b, 20	18, 20, 21, 26	17, 18, 19a, 20, 21, 22a, 22b, 26	16b, 18[b], 21, 22b, 26
19b		2.01 (ddd, 12.2, 7.0, 5.6)[c]	18, 19a, 20	17, 18	16b, 17, 18, 19a, 20, 21, 22a, 26	18, 19a, 20, 22a, 22b, 26
20	83.2 (d)	3.63 (m)	19a, 19b, 21	21, 22	17, 18, 19a, 19b, 21, 22a, 22b, 26	18, 19b, 21[b], 22a, 22b
21	73.0 (d)	3.42 (ddd, 11.1, 8.8, 1.8)	20, 22a, 22b	20, 22, 23	17, 18, 19a, 19b, 20, 22a, 22b, 23, 24a, 24b, 26	13, 16b, 19a, 22a[b], 22b, 23
22a	34.1 (t)	1.46 (ddd, 14.1, 11.1, 1.9)	21, 22b, 23	20, 21	18, 19a, 19b, 20, 21, 22b, 23, 24a, 24b, 26	19b, 21[b], 22b[b], 23, 24a, 24b
22b		1.76 (ddd, 13.9, 11.7, 1.8)	21, 22a, 23	23, 24	19a, 20, 21, 22a, 23,24a, 24b	19a, 19b, 21, 22a[b],23[b], 24a, 24b
23	72.3 (d)	5.23 (dddd, 11.7, 4.9, 2.9, 1.9)	22a, 22b, 24a, 24b	1	21, 22a, 22b, 24a, 24b	21, 22a, 22b[b], 24a, 24b
24a	66.1 (t)	3.61 (m)	23, 24b	22, 23	23, 24b	22a, 22b, 23, 24b
24b		3.81 (dd, 12.2, 2.9)[c]	23, 24a	22, 23	22b, 23, 24a	22a, 22b, 23, 24a
25	18.3 (q)	0.85 (d, 6.6)	11	10, 11, 12	9, 10a, 10b, 11, 12, 13, 14	9, 10a, 10b, 11[b], 12
26	14.5 (q)	1.03 (d, 6.9)	18	17, 18, 19	15, 16a, 16b, 17, 18, 19a, 19b, 20 21	16a, 16b, 18[b], 19a, 19b
1′	94.2 (d)	5.02 (d, 1.1)	2′	7, 2′, 3′, 5′	2′, 6′	6eq, 7, 8eq, 2′, 7′
2′	80.8 (d)	3.40 (dd, 3.8, 1.4)	1′, 3′	3′, 4′, 7′	1′, 3′, 4′, 5′, 6′, 8′, 9′	1′
3′	71.7 (d)	3.68 (m)	2′, 4′, 8′		2′, 4′, 5′, 6′, 8′, 9′	2′, 4′[b]
4′	74.3 (d)	3.34 (dd, 9.4, 9.4)	3′, 5′	3′, 5′, 6′	3′, 5′, 6′, 8′, 9′	3′[b], 5′[b], 6′
5′	68.1 (d)	3.62 (m)	4′, 6′	3′, 4′, 6′	4′, 6′, 8′, 9′	8eq, 4′[b], 6′
6′	17.7 (q)	1.27 (d, 6.3)		4′, 5′	1′, 3′, 4′, 5′, 8′	4′, 5′[b]
7′	59.1 (q)	3.45 (s)		2′		1′
	OH-3′	2.24 (s)	2, 4a, 4b		2′, 3′, 4′, 5′, OH-4′	
	OH-4′	1.54 (s)	2, 3		3′, 4′, 5′, OH-3′	

[a]HMBC correlations are presented from proton to indicated carbon. [b]COSY artifacts observed in ROESY spectrum. [c]$^3J_{HH}$ values obtained from DQFCOSY and/or NMRSim.

The molecular formula of mandelalide D (**4**) was assigned by HR-ESI-MS ($[M + Na]^+$ m/z 659.3424) as $C_{34}H_{52}O_{11}$, implying 9 degrees of unsaturation. Comparison of the similar ^1H NMR spectra (Table 2) for mandelalides C (**3**) and D (**4**) indicated a second aglycone structure. A key difference between the ^1H spectra for the two compounds was the further deshielded H-24 doublet (δ_H 5.17) for **4** relative to that for **3** (δ_H 3.98). In the HMBC spectrum for **4**, the H-24 doublet was correlated to a carbonyl ^{13}C resonance (δ_C 173.1, C-1″), which also showed correlations from H-2a″, H-2b″ and H-3″, consistent with an additional butyrate substituent at C-24. Thus, mandelalide D (**4**) is 24-butyro mandelalide C (**3**). Over a period of 12 months, we observed changes in the ^1H NMR spectrum of **4** that were consistent with the loss of both butyrate moieties, resulting in the new compound deacylman-

dx.doi.org/10.1021/jo3008622 | J. Org. Chem. 2012, 77, 6066−6075

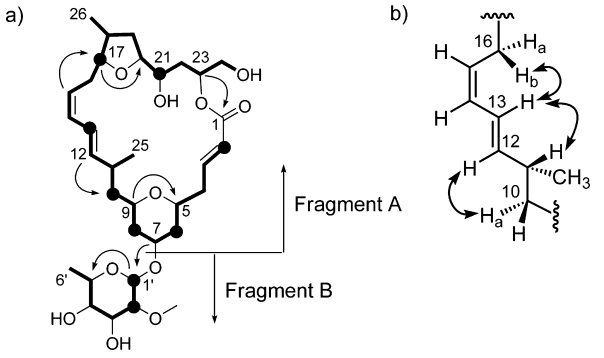

Figure 1. (a) Planar structure of **1** showing TOCSY correlations from H-2, H-6, H-8, H-10b, H-13, H-17, H-21, H-1′, H-2′ (black circles) indicated as bolded lines and key HMBC correlations represented by single-headed arrows. (b) Assignment of geometry around the C-13/C-14 bond in **1** using key ROESY correlations indicated by double-headed arrows.

delalide D (**4b**, *m*/*z* 519.3 [M + Na]$^+$, Table S6, Supporting Information).

Consideration of the differences in the planar macrocyclic structures, and available amounts, of mandelalides A−D (**1**−**4**) lead to the conclusion that the assignment of relative configuration should be performed on mandelalide A and one of mandelalides B−D. Similarities in coupling constant ($^3J_{HH}$) values for mandelalides B−D suggested retention of the relative configuration of the macrocycle between these structures (Table 2). Therefore besides mandelalide A, mandelalide B (**2**) was selected for further analysis because it also possesses a monosaccharide moiety, although it lacks the C-24 chiral center present in **3** and **4**. For both mandelalides A (**1**) and B (**2**), the relative configuration of the macrocycle could be assigned fully using a combination of ROESY and *J*-based configuration analysis of data acquired in $CDCl_3$ and pyridine-d_5, which were consistent between the two solvents.

Considering the tetrahydropyran ring of **1**, ROESY correlations between H-5, H-7 and H-9 supported their axial orientation, consistent with a chair conformation and equatorial C-7 glycosidic bond (Figure 2a). The relative configuration for fragment C-9 to C-11 (−$CHCH_2CH$−) was assigned on the basis of coupling constants obtained from the ^{1}H spectrum and a DQFCOSY. In $CDCl_3$, $^3J_{HH}$ values of 2.2 and 11.2 Hz for H-9/H-10a and H-9/H-10b, respectively, localized H-10a *gauche* and H-10b *anti* to H-9 in two possible rotamers (Figure 2b), the correct one of which should be distinguishable from ROESY data. ^{1}H signal overlap in the $CDCl_3$ ROESY spectrum for mandelalide A (**1**) obscured ROE interactions in the region of interest. However, acquisition of NMR data for **1** in py-d_5 provided sufficient resolution (0.16 ppm, Figure S20, Supporting Information) between H-8_{ax} and H-10a to reveal ROESY correlations between H-8_{ax} and H-10b, and H-8_{eq} and H-10a. This lead to the conclusion that rotamer A is correct, orienting H-10a to the outside of the macrocycle, (Figure 2). The assignment of relative configuration around the C-10/C-11 bond required direct measurement of $^3J_{HH}$ values from DQFCOSY, again due to significant overlap. In $CDCl_3$, $^3J_{HH}$ values of 9.6 Hz for H-10a/H-11 and 3.7 Hz for H-10b/H-11 indicated *anti* and *gauche* orientations, respectively (Figure 2c). Finally, ROESY correlations between H-9 and H_3-25, and H-11 and H-13 were consistent with the relative configuration shown in Figure 2a. This assignment was supported by HETLOC data in $CDCl_3$ (Figures S11, Supporting Information), which provided very weak, but measurable $^3J_{HC}$ between H-10a and C-25 (0.9 Hz), and between H-10b and C-25 (8.9 Hz).

For the tetrahydrofuran ring of **1**, H-17 and H-20 could be in a *cis* or *trans* configuration. There are two close conformational minima (envelope and half-chair) for THF rings.[15] However, in the envelope conformation CH_3-26, H-18, H-19a and H-19b in **1** would be *eclipsed*, while these same moieties would be *gauche* in the half-chair conformation and there would be no eclipsed interaction along the C-18/19 bond.[15] Therefore we decided to analyze ROESY correlations in the context of a half-chair THF ring to assign the relationship of H-17 and H-20. The relatively large $^3J_{HH}$ couplings between vicinal proton pairs H-16b/H-17 (11.4 Hz) and H-20/H-21 (8.8 Hz) supported their *anti* orientation in each case (Figure 3a). Moreover, ROESY correlations between H-16b and H-19a, H-16b and H-21, and H-19a and H-21 were consistent with a *cis* localization of H-17 and H-20 (Figure 3b), despite that no direct ROESY correlation was observed between H-17 and H-20. Instead, the proposed conformation, consistent with ROESY correlations between H_3-26/H_2-16 and H-16b/H-21, brings ROE-correlated H-18 and H-20 into close proximity (Figure 3b). For the C-21 chiral center, the large values of $^3J_{HH}$ and $^2J_{HC}$ (8.8 and −4.0 Hz, respectively), in parallel with the lack of NOE contact between H-20 and H-21 (resolved in py-d_5), are consistent with their *anti* orientation (Figure 3a), as stated above. Analysis of $^3J_{HH}$ between H-21/H-22a (11.1 Hz), and H-21/H-22b (1.8 Hz), placed H-22a *anti* and H-22b *gauche* with respect to H-21 (Figure 3c). ROESY correlations between H-19a and H-22b, H-19b and H-22a, and H-19b and H-22b suggested that H_2-22 are directed away from the center of macrocycle, with the C-21 hydroxyl pointing toward the center. Analogous reasoning was used to resolve the relative configuration at C-23. The respective large and small $^3J_{HH}$ values between H-22b/H-23 (11.7 Hz) and H-22a/H-23 (1.9 Hz) suggested *anti* and *gauche* orientations, respectively (Figure 3d).

Configurational assignment of the mandelalide A monosaccharide (C-1′ to C-6′) relied on $^3J_{HH}$ values, obtained from the ^{1}H NMR and assigned by DQFCOSY, given the overlap for H-3′ to H-5′ signals in both $CDCl_3$ and py-d_5 ROESY spectra. Although the small value of $^3J_{H\text{-}1'/H\text{-}2'}$ = 1.1 Hz was inconclusive, H-2′ was assigned as equatorial based on $^3J_{H\text{-}2'/H\text{-}3'}$ = 3.8 Hz. The H-4′ multiplet indicated couplings of 9.4 Hz with both H-3′ and H-5′, indicative of axial hydrogens, although the direct analysis of H-3′ and H-5′ multiplets was impeded by their overlap with other ^{1}H shifts. Overall, these data for CH-2′ to CH-5′ were consistent with the relative configuration of 2-*O*-methylrhamnose. To confirm this and to assign the monosaccharide as *α*- or *β*-2-*O*-methylrhamnose, we decided to analyze the magnetization transfer pattern of TOCSY signals originating from the anomeric center (C-1′), following the method proposed by Gheysen et al.[16] This "TOCSY matching" approach takes advantage of the fact that the size of the $^3J_{HH}$ scalar couplings affect the rate of magnetization transfer through a ^{1}H spin system during the TOCSY spin-lock period. The acquisition of a TOCSY with a spin-lock of 100 ms (Figure S9, Supporting Information) affords a differential presence or absence of the CH_3-6′ signal in *α*- and *β*-rhamnose, respectively. In the TOCSY acquired for mandelalide A (**1**), the intensity of peaks fit to previously reported data for *α*-rhamnose (Figure S9).[16] Additional confirmation that the monosaccharide attached to **1** is 2-*O*-methyl-*α*-rhamnose was provided by the measurement of $^1J_{HC}$ = 167.2 Hz for the anomeric CH-1′ from

dx.doi.org/10.1021/jo3008622 | J. Org. Chem. 2012, 77, 6066−6075

Table 2. ^{1}H and ^{13}C NMR Data for Mandelalides B–D (2–4) in $CDCl_3$

	Mandelalide B (2)		Mandelalide C (3)		Mandelalide D (4)	
no.	δ_C (mult)	δ_H (J in Hz)	δ_C (mult)	δ_H (J in Hz)	δ_C (mult)	δ_H (J in Hz)
1	175.6 (s)		174.7 (s)		172.9 (s)	
2	79.3 (s)		82.0 (s)		81.3 (s)	
3	69.5 (d)	5.48 (dd, 6.0, 1.7)	68.3 (d)	5.51 (dd, 6.6, 0.9)	68.6 (d)	5.56 (dd, 6.6, 0.7)
4a	36.3 (t)	1.59 (m)	36.4 (t)	1.65 (m)	36.2 (t)	1.68 (m)
4b		2.14 (ddd, 15.0, 11.7, 1.5)		2.14 (ddd, 15.6, 11.7, 1.0)		2.18 (ddd, 15.4, 11.5, 0.9)
5	72.7 (d)	3.30 (dddd, 11.4, 11.4, 1.5, 1.5)	72.3 (d)	3.25 (dddd, 11.4, 11.4, 1.8, 1.8)	72.2 (d)	3.21 (dddd, 11.2, 11.2, 1.3, 1.3)
6ax	37.4 (t)	1.10 (ddd, 11.7, 11.7, 11.7)	41.2 (t)	1.11 (ddd, 12.5, 11.4, 11.4)	41.2 (t)	1.12 (ddd, 11.3, 11.3, 11.3)
6eq		1.89 (m)		1.86 (m)		1.85 (dddd, 12.2, 4.6, 1.5, 1.5)
7	73.3 (d)	3.75 (m)	68.3 (d)	3.76 (dddd, 10.9, 10.9, 4.6, 4.1)	68.4 (d)	3.75 (m)
8ax	39.6 (t)	1.23 (m)	41.8 (t)	1.13 (ddd, 12.5, 11.2, 11.2)	41.8 (t)	1.12 (ddd, 11.3, 11.3, 11.3)
8eq		1.81 (dddd, 12.4, 4.8, 1.8, 1.8)		1.83 (m)		1.83 (dddd, 12.2, 4.6, 1.5, 1.5)
9	72.4 (d)	3.39 (dddd, 11.0, 11.0, 2.2, 2.2)	72.3 (d)	3.37 (dddd, 10.9, 10.9, 2.1, 2.1)	72.2 (d)	3.36 (dddd, 11.0, 11.0, 2.2, 2.2)
10a	42.2 (t)	1.18 (ddd, 14.1, 12.3, 2.8)	42.1 (t)	1.19 (ddd, 14.2, 12.1, 2.8)	42.1 (t)	1.19 (ddd, 13.9, 11.5, 2.8)
10b		1.57 (m)		1.57 (m)		1.57 (ddd, 14.0, 11.5, 4.0)
11	33.9 (d)	2.50 (m)	34.0 (t)	2.49 (m)	34.2 (d)	2.48 (m)
12	142.1 (d)	5.50 (dd, 15.1, 9.8)	142.2 (d)	5.50 (dd, 14.6, 9.6)	142.3 (d)	5.50 (dd, 14.8, 9.7)
13	123.3 (d)	6.40 (dd, 14.7, 11.3)	123.2 (d)	6.39 (dd, 14.6, 11.4)	123.1 (d)	6.38 (dd, 15.0, 11.3)
14	131.0 (d)	6.10 (dd, 11.1, 11.1)	131.1 (d)	6.10 (dd, 11.0, 11.0)	131.1 (d)	6.10 (dd, 11.0, 11.0)
15	127.1 (d)	5.28 (ddd, 11.1, 11.1, 5.2)	127.1 (d)	5.28 (ddd, 11.0, 11.0, 5.4)	127.1 (d)	5.28 (ddd, 11.3, 11.3, 5.4)
16a	30.7 (t)	1.90 (m)	30.7 (t)	1.90 (ddd, 13.6, 5.2, 1.1)	30.6 (t)	1.90 (ddd, 13.6, 5.3, 1.0)
16b		2.31 (ddd, 13.6, 11.6, 11.5,)		2.30 (ddd, 13.8, 11.9, 11.9)		2.29 (ddd, 13.1, 11.3, 11.3)
17	81.5 (d)	3.95 (ddd, 11.6, 7.46, 1.6)	81.6 (d)	3.95 (ddd, 11.5, 7.5, 1.1)	81.6 (d)	3.94 (ddd, 12.0, 7.5, 1.1)
18	38.3 (d)	2.52 (m)	38.3 (d)	2.53 (m)	38.3 (d)	2.54 (dddq, 12.3, 7.5, 7.02, 6.8)
19a	35.6 (t)	1.33 (ddd, 12.2, 12.2, 8.2)	35.7 (t)	1.33 (ddd, 12.2, 12.2, 9.1)	35.7 (t)	1.34 (ddd, 12.3, 12.3, 9.2)
19b		2.05 (ddd, 12.8, 6.9, 6.9)		2.10 (ddd, 12.5, 7.0, 6.8)		2.08 (ddd, 12.2, 7.02, 7.02)
20	82.1 (t)	3.77 (m)	82.4 (d)	3.82 (ddd, 9.2, 9.2, 7.0)	82.2 (d)	3.79 (ddd, 9.3, 9.3, 7.0)
21	74.5 (d)	3.76 (m)	74.4 (d)	3.73 (ddd, 10.8, 9.5, 1.2)	74.3 (d)	3.73 (ddd, 10.0, 10.0, 1.6)
22a	37.9 (t)	1.51 (m)	32.1 (t)	1.59 (m)	32.5 (t)	1.47 (ddd, 14.2, 10.5, 1.0)
22b		1.64 (m)		1.82 (ddd, 14.4, 11.0, 1.0)		1.65 (m)
23	74.9 (d)	4.84 (dddd, 10.4, 10.4, 4.9, 1.0)	78.9 (d)	5.01 (ddd, 11.2, 2.0, 2.0)	76.7 (d)	5.13 (ddd, 10.8, 3.3, 0.8)
24a	39.7 (t)	1.93 (dd, 12.7, 10.7)	72.2 (d)	3.98 (d, 2.8)	74.0 (d)	5.17 (d, 3.3)
24b		2.39 (dd, 12.8, 4.9)				
25	18.5 (q)	1.07 (d, 6.6)	18.4 (q)	1.06 (d, 6.2)	18.3 (q)	1.07 (d, 6.6)
26	14.2 (q)	1.03 (d, 6.9)	14.2 (q)	1.03 (d, 6.9)	14.3 (q)	1.04 (d, 6.8)
	OH-21	2.70 (br s)	OH	2.80 (br s)	OH	2.71 (br s)
	OH-2	2.87 (s)			OH	2.78 (br s)
1′	94.8 (d)	5.04 (s)	173.4 (s)		173.6 (s)	
2′a	80.9 (d)	3.33 (ddd, 3.0, 1.5. 1.3)	36.3 (t)	2.34 (td, 7.5, 1.2)	36.3 (t)	2.40 (dt, 15.5, 7.3)
2′b						2.43 (dt, 15.5, 7.3)
3′	66.6 (d)	3.74 (m)	18.7 (t)	1.65 (m)	18.6 (t)	1.70 (m)
4′	73.3 (d)	3.49 (ddt, 11.8, 3.3, 1.2, 1.2)	13.9 (q)	0.94 (t, 7.5)	13.9 (q)	0.96 (t, 7.4)
5′	67.4 (d)	3.85(br q, 6.6)				
6′	16.6 (q)	1.23 (d, 6.5)				
7′	59.6 (q)	3.45 (s)				
	OH-3′	2.86 (d, 11.6)				
	OH-4′	2.74 (d, 11.6)				
1″	173.6 (s)				173.1 (s)	
2″a	36.3 (t)	2.35 (t, 7.5)			36.0 (t)	2.31 (dt, 12.8, 7.5)
2″b						2.33 (dt, 12.8, 7.5)
3″	18.8 (t)	1.67 (tq, 7.4, 7.4)			18.6 (t)	1.63 (m)
4″	14.0 (q)	0.95 (t, 7.4)			13.8 (q)	0.93 (t, 7.3)

a HETLOC experiment (Figure S12, Supporting Information). This value is in agreement with that reported previously for 2-*O*-methyl-α-rhamnose, although is smaller than in the case of nonmethylated common sugars (~170 Hz).[17,18]

As in the case of **1**, the coupling constants values and ROESY correlations measured from both $CDCl_3$ and py-d_5 data for mandelalide B (**2**) were comparable, indicating similar conformations in both solvents. The chair conformation of the THP ring in **2** (C-5 to C-9) was confirmed by the presence of diaxial ROESY correlations between H-5, H-7 and H-9 (Figure 4a). For the C-9/C-11 segment, coupling constants of 2.2 and 11 Hz, between H-9/H-10a, and H-9/H-10b confirmed *gauche* and *anti* relationships, respectively. Similarly for H-10a/H-11 and H-10b/H-11, large (12.3 Hz) and small (4.1 Hz in

dx.doi.org/10.1021/jo3008622 | J. Org. Chem. 2012, 77, 6066–6075

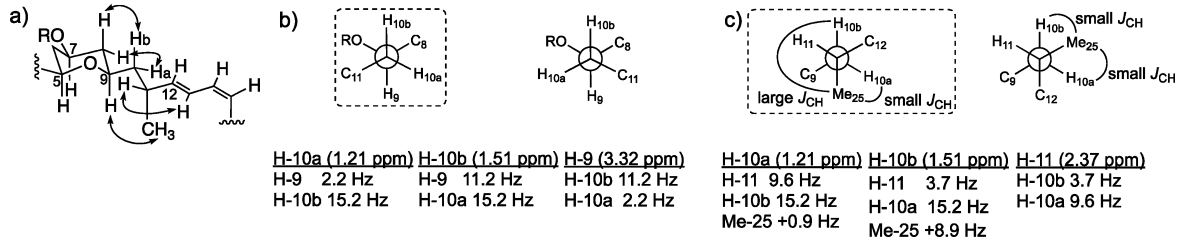

Figure 2. (a) Key ROESY correlations indicated on the C-5/C-15 fragment of **1**. (b) Two possible rotamers around the C-9/C-10 bond. (c) Most feasible rotamers around the C-10/C-11 bond of **1**, with anticipated large/small heteronuclear coupling constant indicated on each. For b and c, the J_{HH} and J_{HC} values ($CDCl_3$) are listed below the Newman projections and the rotamer of best fit is indicated by a dashed outline.

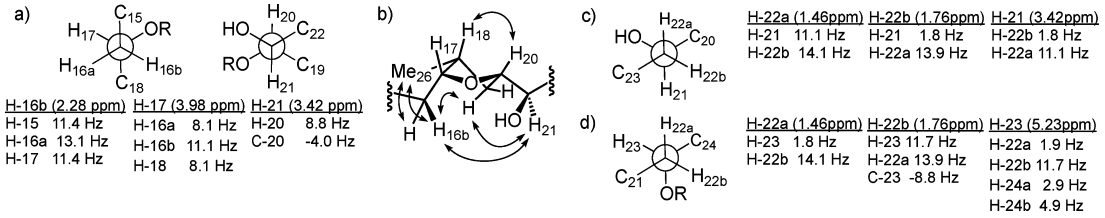

Figure 3. (a) Newman projections along the C-16/C-17 and C-20/C-21 bonds in **1**. (b) The most feasible *cis* orientation of the THF ring with double-headed arrows indicating ROESY correlations. (c) Newman projection along the C-21/C-22 bond with applicable J_{HH} and J_{HC} values ($CDCl_3$) indicated on the right. (d) Newman projection along the C-22/C-23 bond and relevant coupling constants.

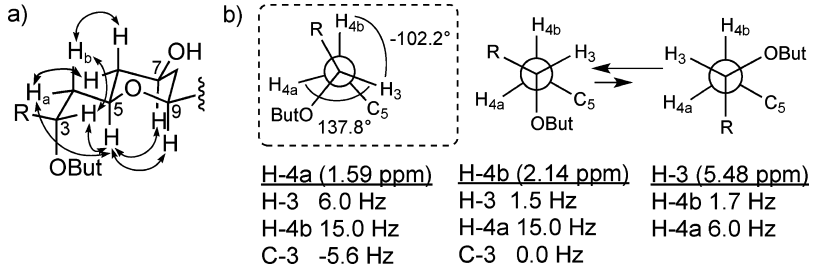

Figure 4. (a) Key ROESY correlations for the C-3/C-5 fragment are indicated by double-headed arrows on the partial structure. (b) The most probable rotamer along the C-3/C-4 bond highlighted by the dashed outline and alternative equilibrium of two rotamers explaining medium size coupling constants. But = butyrate.

$CDCl_3$, 3.8 Hz in py-d_5) coupling constants assigned from DQFCOSY supported *anti* and *gauche* relationships, respectively, overall leading to the same relative configuration in this region as for **1**. For the C-3/C-5 fragment of **2**, $^3J_{HH}$ values of 1.5 and 11.7 Hz between H-4a/H-5 and H-4b/H-5 supported *gauche* and *anti* orientations, respectively. A small coupling of 1.6 Hz between H-3 and H-4b indicated their *gauche* relationship (Figure 4b), and was in agreement with large H-4a/C-3 (−5.6 Hz) and small H-4b/C-3 (0 Hz) heteronuclear couplings. However, medium couplings for H-3/H-4a (6.0 Hz) and H-5/C-3 (4.3 Hz) suggested that the staggered orientation along C-3/4 may be distorted or that more than one conformation is present along this bond. Clear ROESY correlations between H-3 and each of H-4b, H-5, H-9, H-11, H-23 and H-24b, but not H-4a (apparent COSY artifact only), support a distorted rotamer in which 138° and −102° angles are present between H-3/H-4a and H-3/H-4b, as calculated using MestReJ for $^3J_{HH}$ 6.0 and 1.6 Hz respectively (Figure 4b).

The presence of a ROESY correlation between H-18 and H-20 on the THF ring in mandelalide B (**2**) placed CH_3-26 quasi-equatorial, consistent with ROESY correlations from the latter methyl to H_2-16, (as for **1**, Figure 3). ROESY correlations (Table S2, Supporting Information) and comparative analysis of coupling constant values (Table 2) around the C-16/C-21 fragment confirmed that a *cis* conformation of the THF ring is conserved in mandelalides A (**1**) and B (**2**).

Given extensively overlapped $CDCl_3$ ^{1}H chemical shifts for the C-20/C-23 fragment in **2**, analysis of ^{1}H NMR and DQFCOSY in py-d_5 was used to assign the relative configuration of this region. The $^3J_{HH}$ values for **2** were similar to those for mandelalide A (**1**), despite the presence of the γ-lactone ring in **2**. However, in contrast to **1**, in which the more shielded H-22a (δ 1.46) is *anti* to H-21 and *gauche* to H-23 (Figure 3), for **2** the more shielded H-22a (δ 1.65) is *gauche* to H-21 ($^3J_{HH}$ < 1 Hz) and H-22b (δ 1.77) is *anti* to H-21 ($^3J_{HH}$ = 9.4 Hz), while H-20 and H-21 remain *antiperiplanar* ($^3J_{HH}$ = 9.4 Hz) (Figure 5a). Coupling constant values obtained directly from the oxymethine H-23 multiplet, and assigned by DQFCOSY, indicate *anti* relationships with H-22a (J_{HH} =

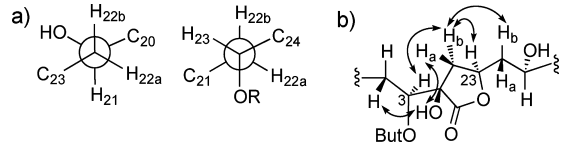

Figure 5. (a) Assigned rotamers along the C-21/C-22 and C-22/C-23 bonds in **2**. (b) ROESY correlations around the γ-butyrolactone of **2**. But = butyrate.

dx.doi.org/10.1021/jo3008622 | J. Org. Chem. 2012, 77, 6066−6075

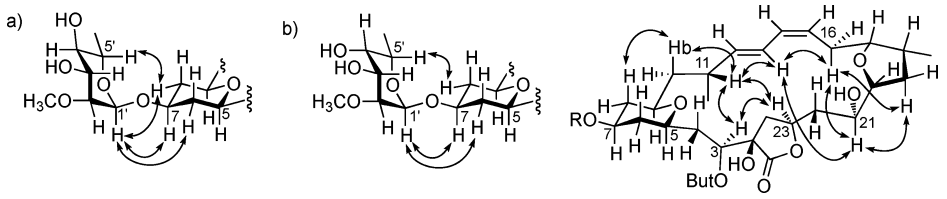

Figure 6. (a) Key ROE correlations ($CDCl_3$) between the monosaccharide and the macrolide THP moiety in mandelalide A. (b) Key ROE correlations between the monosaccharide and the macrolide, as well as through ring correlations for mandelalide B.

11.2 Hz), and a *gauche* relationship with H-22b (J_{HH} = 1.0 Hz). The orientation of the ester bond in the butyrolactone ring could be assigned knowing the localization of H-23 *anti* to H-22a. The ester oxygen must then be positioned *gauche* or *anti* to H-22b. The ROEs observed between H-24a, H-24b and H-22b in py-d_5, in parallel with the absence of ROEs between H_2-24 and H-21 suggested that the ester bond is *anti* to H-22b (Figure 5a). Finally, knowing the relative configuration of the C-3/C-11 and C-20/C-23 fragments, the chirality of the quaternary C-2 in the butyrolactone ring was considered. ROESY correlations between H-24b and both H-3 and H-23 were consistent with an α-oriented H-24b, while H-24a, showing ROESY correlations to H_2-22, is oriented above the butyrolactone ring in a β configuration. Similarly, the C-2 hydroxyl could be oriented to the outside of the macrocycle due to the presence of weak ROESY signals between this OH-2 and H-4b and H-24a, suggesting a 2*R* configuration (Figure 5b).

The relative configuration of the 2′-*O*-methyl, 6′-deoxy monosaccharide moiety (C1′−C7′) in **2** was established analogously to that in **1**. A very weak ROESY correlation (py-d_5) between H-1′ and H-5′ together with $^1J_{HC}$ = 167 Hz for anomeric CH-1′ suggested the presence of an α-sugar. A ROESY correlation between H-3′ and H-5′ localized these protons axial, while the small $^3J_{HH}$ between H-2′ and H-3′, (2.8 Hz) localized H-2′ equatorial (Figure 6). The presence of a W coupling ($^4J_{HH}$ = 0.98 Hz) between H-2′ and H-4′, as well as $^3J_{HH'}$ = 3.2 Hz between H-3′ and H-4′ localized H-4′ equatorial, overall leading to the conclusion that mandelalide B (**2**) contains 2-*O*-methyl-6-dehydro-α-L-talose, the C-4′ epimer of the monosaccharide in mandelalide A.

Given the assignment of relative configuration of the macrocycle and monosaccharide units of mandelalides A (**1**) and B (**2**), it remained to establish the absolute configuration of these glycosidic macrolides. Despite our desire to conserve the limited sample quantities available for further biological investigations, a chemical degradation/derivatization approach to the absolute configuration would be most rigorous and was facilitated by the contiguous nature of the stereogenic fragments throughout the molecular framework. Importantly, inspection of the $CDCl_3$ and py-d_5 ROESY spectra for **1** and **2** revealed clear correlations between protons of the monosaccharide and THP of the macrocycle (Figure 6a, b). Given the well-defined solution structures of monosaccharides and glycosidic bond conformations,[19] assignment of the rhamnose absolute configuration would permit subsequent relay of configurational assignments around the macrocycle, as shown for mandelalide B (Figure 6b). Therefore, a portion (100 μg) of mandelalide A (**1**) was sacrificed for hydrolysis of the glycosidic bond and chiral GC-MS comparison of the liberated derivatized monosaccharide with permethylated and silylated D- and L-rhamnose standards. During coinjection of each standard with the derivatized natural product hydrolysate, the natural product sugar coeluted with the L (97.4 min) and not the D (96.4 min) synthetic standard, confirming that the sugar substituent of **1** is 2-*O*-methyl-α-L-rhamnose. The absolute configuration of this sugar could then be extrapolated to the aglycone of **1** based on the ROESY correlations between H-1′ and H-7, H-1′ and H-6_{eq}, and H-5′ and H-8_{eq} to provide an assignment of the mandelalide A (**1**) aglycone as 2*E*, 5*S*, 7*S*, 9*R*, 11*R*, 12*E*, 14*Z*, 17*R*, 18*R*, 20*R*, 21*R*, 23*R*. Given retention of the macrocycle configuration (C-5 to C-21) between **1** and **2**, the absolute configuration of **2** could be assigned similarly by considering ROESY correlations between the monosaccharide and THP moiety, and key correlations across this more rigid macrocycle (Figure 6b). Thus the aglycone of mandelalide B (**2**) could be assigned as 2*R*, 3*R*, 5*R*, 7*S*, 9*R*, 11*R*, 12*E*, 14*Z*, 17*R*, 18*R*, 20*R*, 21*R*, 23*R*.

Computational modeling of mandelalide B was used to examine possible mandelalide B conformations (Figure 7). An attempt to investigate the fit of calculated conformations to experimental data was based on measurements of ROE distances across the macrocycle in py-d_5.[20] However, as could be expected for a flexible macrolide, for the ten lowest energy conformations of mandelalide B (**2**), the differences between the calculated and experimental average distances between all analyzed protons except H-21/H-11 and H-21/H-13 were significantly different (0.2 Å or more). Nevertheless, the lowest energy computational model assists in visualizing the through ring ROE contacts that facilitated assignment of the absolute configuration (Figure 7).

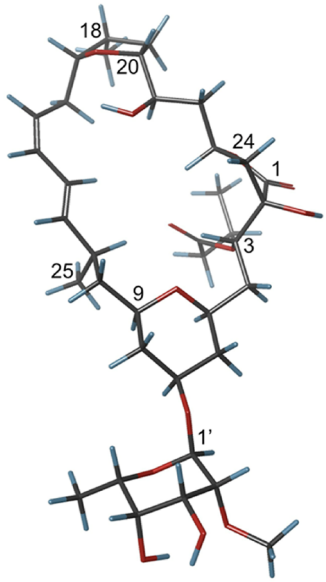

Figure 7. Computational model of the lowest energy conformer for mandelalide B (**2**).

dx.doi.org/10.1021/jo3008622 | J. Org. Chem. 2012, 77, 6066−6075

The $^3J_{HH}$ values acquired in $CDCl_3$ for mandelalides B−D (**2**−**4**) were all similar, suggesting that the relative configuration of the macrocycle incorporating a γ-butyrolactone is retained. The configuration at the remaining C-24 stereocenter present in mandelalides C (**3**) and D (**4**) was assigned from ROESY data. In each case, the H-24 doublet (δ_H 3.98 and 5.17 in **3** and **4**, respectively) is correlated to the H-3 double doublet, localizing the C-24 hydroxyl/butyrate moiety antiperiplanar to H-3 and H-23, in an *S* configuration.

Cytotoxicity of the organic extract from *Lissoclinum* sp. was examined against mouse Neuro-2A neuroblastoma, and human MDA-MB-231 breast and NCI-H460 lung cancer cell lines following 48 h exposure. In all cases low μg/mL IC_{50} values were obtained (Table 3). The Neuro-2A cell line was chosen to perform activity-guided fractionation leading to the purification of mandelalides A−D (**1**−**4**). The pure compounds mandelalides A and B yielded nanomolar IC_{50} values against Neuro-2A (44.0 and 83.8, respectively) and NCI-H460 (12.0 and 29.4, respectively) cell lines (Table 3, Figure S57, Supporting Information). The potent cytotoxicities of these mandelalides are somewhat surprising given the reported minimal cytotoxicity of the related glycosylated polyketides madeirolides A and B.[21] The latter metabolites caused less than 50% inhibition of AsPC-1 and PANC-1 pancreatic cancer cells at 10 μg/mL, but showed potent fungicidal activity against *Candida albicans*. Madeirolides A and B share essentially the same western hemisphere of the mandelalides (C-5 to C-22), including a THP (alternatively substituted), diene, THF and neighboring hydroxymethine. The two series of compounds vary only in the closure of the macrocycle: the position of the lactone and additional cycle. Given that the madeirolides were isolated from a deep-water lithistid *Leiodermatium* sponge, their structural relatedness is consistent with a microbial biogenetic origin. Side-by-side evaluation of the biological properties of all four mandelalides and the two madeirolides would provide insight into the structure−activity relationships that result in potent cytotoxicity and fungicidal activity, respectively. However, the inaccessible supply of both source organisms means that further investigation of these metabolites will likely await their total syntheses.

Table 3. Cytotoxicity of *Lissoclinum* sp. Organic Extract and Mandelalides A (1) and B (2) to Mouse Neuro-2A Neuroblastoma and Human NCI-H460 Lung and MDA-MB-231 Breast Cancer Cells

	IC_{50} (at 48 h) in Cancer Cell Lines[a]		
	NCI-H460	Neuro-2A	MDA-MB-231
organic extract	0.7 μg/mL	5.6 μg/mL	22.1 μg/mL
mandelalide A (**1**)	12 nM	44 nM	
mandelalide B (**2**)	29 nM	84 nM	

[a]Cell viability was assessed by MTT assay and IC_{50} values were derived using nonlinear regression analysis.

EXPERIMENTAL SECTION

General Experimental Methods. As described previously.[22] Additionally NMR data in $CDCl_3$ were acquired at 700 (^{1}H) and 175 (^{13}C) MHz on a 5 mm inverse cryogenic probe. The NMR data in py-d_5, TOCSY (mixing time 100 ms), HETLOCs and gated-decoupled ^{13}C NMR experiments were obtained at 700 (^{1}H) and 175 (^{13}C) MHz on a 5 mm ^{13}C cryogenic probe. The spectra were referenced to internal residual solvent signals in ppm (^{1}H NMR: $CDCl_3$, 7.24, py-d_5, 8.74, CD_3OD, 3.31; ^{13}C NMR: $CDCl_3$, 77.23, py-d_5, 150.35, CD_3OD, 49.15). High-resolution MS data were acquired using an orthogonal acceleration time-of-flight (oa-TOF) mass analyzer and electrospray ionization (ESI).

Extraction and Isolation. The ascidian, *Lissoclinum* sp. (Ascidiacea, Aplousobranchia, Didemnidae) was collected by hand using SCUBA at a depth of 18 m (July 20, 2004) from White Sands Reef in Algoa Bay, Eastern Cape Province, South Africa (33:59.916S, 25:42.573W). The type specimen (SAF2004-55) for this new ascidian species is housed at the South African Institute for Aquatic Biodiversity (SAIAB), Grahamstown, South Africa.

The freeze-dried organism (15.1 g) was extracted with 2:1 CH_2Cl_2-MeOH yielding 1.45 g of organic extract. This organic extract was fractionated on Sephadex LH-20 (CH_2Cl_2−MeOH, 1:3) to give eight fractions, of which fractions six and seven were subjected to reversed phase C_{18} solid phase extraction (RP-SPE) using a stepped gradient of 50−100% MeOH in H_2O. The 75% MeOH-H_2O and 100% MeOH fractions were further separated by RP-HPLC (C_{18} column, 250 mm × 10 mm, 7:3 MeOH-0.1% FA in H_2O) to yield mandelalides A (**1**, 0.8 mg), B (**2**, 0.5 mg), C (**3**, 0.8 mg) and D (**4**, 0.6 mg).

*Mandelalide A (**1**).* Amorphous solid; $[\alpha]^{23}_D$ −9 (*c* = 0.25, MeOH); UV (MeOH) λ_{max} (log ε) 279 (2.7), 217 (4.1); LR-ESI-MS *m*/*z* [M + Na]$^+$ 647.4; HR-ESI-MS *m*/*z* [M+Na]$^+$ 647.3394, (calcd for $C_{33}H_{52}O_{11}Na$, 647.3407); ^{1}H and ^{13}C NMR, COSY, HMBC, TOCSY, ROESY (Tables 1, S1, Supporting Information).

*Mandelalide B (**2**).* Amorphous solid; $[\alpha]^{24}_D$ −13 (*c* = 0.5, MeOH); UV (MeOH) λ_{max} (log ε) 279 (3.0), 229 (4.1); LR-ESI-MS *m*/*z* [M + Na]$^+$ 733.5; HR-ESI-MS *m*/*z* [M + Na]$^+$ 733.3773, (calcd for $C_{37}H_{58}O_{13}Na$, 733.3775); ^{1}H and ^{13}C NMR, COSY, HMBC, ROESY (Tables 2, S2, S3, Supporting Information).

*Mandelalide C (**3**).* Amorphous solid; UV (MeOH) λ_{max} (log ε) 280 (2.7), 229 (4.0); LR-ESI-MS *m*/*z* [M + Na]$^+$ 589.5; HR-ESI-MS *m*/*z* [M + Na]$^+$ 589.2970, (calcd for $C_{30}H_{46}O_{10}Na$, 589.2989); ^{1}H and ^{13}C NMR, COSY, HMBC, TOCSY, ROESY (Tables 2, S4, Supporting Information).

*Mandelalide D (**4**).* Amorphous solid; $[\alpha]^{25}_D$ −50 (*c* = 0.2, MeOH); UV (MeOH) λ_{max} (log ε) 280 (2.7), 229 (4.0); LR-ESI-MS *m*/*z* [M + Na]$^+$ 659.5; HR-ESI-MS *m*/*z* [M + Na]$^+$ 659.3424, (calcd for $C_{34}H_{52}O_{11}Na$, 659.3407); ^{1}H and ^{13}C NMR, COSY, HMBC, TOCSY, ROESY (Tables 2, S5, Supporting Information).

*Deacylmandelalide D (**4b**).* Amorphous solid; $[\alpha]^{27}_D$ −10 (*c* = 0.2, MeOH); UV (MeOH) λ_{max} (log ε) 280 (2.8), 227 (3.8); LR-ESI-MS *m*/*z* [M + Na]$^+$ 519.3; HR-ESI-MS *m*/*z* [M + H]$^+$ 497.2752, (calcd for $C_{26}H_{41}O_9$, 497.2751); ^{1}H and ^{13}C NMR, COSY, HMBC (Table S6, Supporting Information).

Measurement of $^{1,2}J_{HC}$ Coupling Constants. The sensitivity and gradient-enhanced HETLOC (ω1-hetero half-filtered TOCSY) experiment was employed to measure J_{HC} coupling constants, with DIPSI-2 spin-lock set to 60 ms.[23] Spectral widths of 6229 and 5597 Hz, with a data matrix of 4K (F2) × 128 (F1), and 146 or 96 scans were employed in py-d_5 and $CDCl_3$, respectively for mandelalide A. In the case of mandelalide B, a spectral width of 5597 Hz with a data matrix of 4K (F2) × 128 (F1) and 136 scans were implemented in $CDCl_3$. The 1D spectra that were obtained after extraction of F2/F1 slices were subjected to inverse Fourier transform. The resulting FIDs were multiplied by the exponential window function prior to linear prediction processing.[24]

TOCSY Data Acquisition. To determine the magnetization transfer pattern in 2-*O*-methyl-L-rhamnose a 2D TOCSY was acquired with a DIPSI-2 spin-lock sequence in $CDCl_3$. The spectra were recorded with a spin-lock mixing time of 100 ms, 5597 Hz spectral width at 2K (F2) × 512 (F1) data matrix for 40 scans. Data were processed with a sine-bell squared function with 1.5 Hz (F2) and 0.3 Hz (F1) line broadening before measurement of the absolute volumes of peaks. The following designation was applied to depict intensity of peaks; gray ovals indicate intensity or signal greater than 1.5% of intensity measured for the signal of the anomeric proton, white ovals indicate intensity of at least 0.5% but no more than 1.5% intensity measured for the anomeric ^{1}H signal.[16]

dx.doi.org/10.1021/jo3008622 | J. Org. Chem. 2012, 77, 6066−6075

Calculation of Dihedral Bond Angles in MestReJ.[25] The calculation of angles between H-3/H-4a and H-3/H-4b was performed using the Altona equation with substituents at C-3 defined as CH_2OR and OCOR, and substituents at C-4 as H and CH_2OR. Resulting $^3J_{HH}$ values for H-3/H-4a (138.7°) and H-3/H-4b (−102.2°) were 6.0 and 1.6 Hz, respectively.

Computational Modeling of Mandelalide B (2). Computational modeling was performed using the 2009 version of a contemporary software package. Minimization using the Amber* force field with PRCG algorithm, in pyridine (ε = 12.9, 10000 steps, maximum derivative less than 0.05 kcal/mol) and constrained torsion angles H-3/H-4a (138°), H-3/H-4b (−102.2°), H-4b/H-5, H-9/H-10b, H-20/H-21, H-21/H-22b, H-22a/H-23 and distance H-4b/H-24b = 5 Å was first performed. All torsions were restrained based on the $^3J_{HH}$ coupling constants values. The minimized structure was subjected to conformational search using Amber* force field via the low mode sampling method with an energy cut off of 21 kJ/mol and 1000 steps (100 steps per rotatable bond).[26,27] Torsion restraints H-3/H-4a (138°), H-3/H-4b (−102.2°), H-4b/H-5, H-9/H-10b, H-20/H-21, H-21/H-22b, H-22a/H-23 were applied to obtain ground state conformations. Optimization of the ten lowest energy conformations using DFT with the B3LYP functional and 6-31G** basis set in the gas phase resulted in the structure presented in Figure 7.

Methanolysis of Mandelalide A (1). Compound **1** (0.1 mg) was treated with 1 N methanolic HCl (1.0 mL) and heated for 24 h at 70 °C with stirring. The mixture was concentrated *in vacuo*, redissolved in 0.75 mL of 1-(TMS)-imidazole/py (1:4) and the reaction was continued for 40 min at 70 °C with stirring.[28] The solution was concentrated, the final residue partitioned between CH_2Cl_2 and H_2O (1:1), and the organic fraction used for GC-MS analysis.

Preparation of 1,2-Di-*O*-methyl-3,4-di-*O*-TMS-α-L-rhamnose and 1,2-Di-*O*-methyl-3,4-di-*O*-TMS-α-D-rhamnose Standards. L-rhamnose (50 mg) was dissolved in 1N methanolic HCl, heated for 24 h at 70 °C with stirring, and concentrated *in vacuo*. The residue was redissolved in dioxane (0.6 mL) and 2 M TMS-diazomethane in diethyl ether (1.5 mL) was added, with H_3BO_3 as catalyst. The solution was maintained at room temperature with stirring for 5 h and then evaporated to dryness *in vacuo*.[29] Column chromatography on Si gel GF (15 μm) with 5% MeOH in CH_2Cl_2 as mobile phase afforded a 1:3 mixture of 1,2-di-*O*-methyl-α-L-rhamnose and 1,3-di-*O*-methyl-α-L-rhamnose in ∼65% yield from this rate limiting reaction: equivalent to ∼16% yield of the desired 1,2-di-*O*-methyl-α-L-rhamnose to be carried forward for silylation. This 1:3 mixture of methylation products was treated with 1-(TMS)-imidazole/py (1:4) for 40 min at 60 °C and concentrated *in vacuo*.[28] Finally, the residue was dissolved in CH_2Cl_2, loaded on a Si gel column, washed with 100% hexanes, and eluted with 3% EtOAc in hexanes to obtain pure 1,2-di-*O*-methyl-3,4-di-*O*-TMS-α-L-rhamnose in a final yield of 5.4%. The same procedure was applied to produce 1,2-di-*O*-methyl-3,4-di-*O*-TMS-α-D-rhamnose in 6.4% yield. ^{1}H NMR (700 MHz, $CDCl_3$): δ 0.12 (s, 9H), 0.15 (s, 9 H), 3.31 (s, 3H), 3.32 (dd, J = 1.7, 3.2 Hz, 1H), 3.48 (s, 3H), 3.52 (m, 1H), 3.53 (m, 1H), 3.78 (dd, J = 3.6, 8.4 Hz, 1H), 4.61 (d, J = 1.3, 1H); ^{13}C NMR (175 MHz, $CDCl_3$): δ 0.7, 1.2, 18.5, 54.8, 60.0, 69.1, 73.1, 74.3, 81.6, 98.8, ppm; CI-LR-MS: m/z 305 calculated for oxonium ion $C_{13}H_{29}O_4Si_2$.

Absolute Configuration of 2-*O*-Methyl-α-rhamnose from Mandelalide A (1). Analyses of the synthetic standards and permethylated and silylated mandelalide A hydrolysate were performed by GC-MS using a 30 m × 0.25 mm i.d. Cyclosil-B column, and electron impact (EI) ionization. The injector and detector were operated at 250 °C, while the temperature gradient was set to 75−175 °C at 0.5°/min. The retention times for 1,2-di-*O*-methyl-3,4-di-*O*-TMS-α-D-rhamnose and 1,2-di-*O*-methyl-3,4-di-*O*-TMS-α-L-rhamnose injected separately were 96.5 and 98.3 min, respectively. The retention time for the monosaccharide in the derivatized mandelalide A hydrolysate injected separately was 97.5 min. (Figure S56, Supporting Information). Therefore coinjection of the natural product hydrolysate with each standard was performed, yielding two peaks with retention times of 96.4 and 97.4 min, which is indicative of the L-glycoside in mandelalide A (Figure S56, Supporting Information).

Cell Viability Assays. Cytotoxicity of the organic extract and crude fractions was evaluated in mouse Neuro-2A neuroblastoma, and human MDA-MB-231 breast and NCI-H460 lung cancer cells (ATCC, Manassas, VA) using a previously described protocol subjected to slight modifications.[22] Cells were seeded into 96-well plates (20000 cells per well for MDA-MB-231 and NCI-H460, 25000 cells per well for Neuro-2A) in 50 μL of medium 12 hours before treatment. Each test sample was added in a 25 μL aliquot generated by serial dilution in serum-free medium on the day of the experiment, after prior removal of 25 μL of media from the treated well. Aliquots were generated from stock solutions of 6 mg/mL compound in 100% DMSO. Pure compounds **1** and **2** were evaluated in Neuro-2A and NCI-H460 cells after 48 h treatment, as described above. Each compound was tested at final concentrations ranging from 0.001 to 10 μg/mL. In all cases, cell viability was determined after 48 h treatment using a standard 3-(4,5-dimethylthiazol-2-yl)-2,5,diphenyl tetrazolium bromide (MTT) assay.[22] The cytotoxicity of each pure compound was assessed in at least three independent cultures with the viability of vehicle-treated control cells defined as 100% in all experiments. Dose response curves (Figure S57, Supporting Information) were plotted using contemporary biostatistics and curve fitting software.

■ ASSOCIATED CONTENT

Ⓢ Supporting Information

Tables of 1D and 2D NMR data and NMR spectra for compounds **1**−**3** in $CDCl_3$ and py-d_5, for compound **4** in $CDCl_3$, for compound **4b** in CD_3OD. Computational data for mandelalide B (**2**). GC-MS chromatograms for derivatized α-L- and α-D-rhamnose standards and mandelalide A hydrolysate. Dose response curves for mandelalides A and B (**1** and **2**) in Neuro-2A and NCI-H460 cell lines. This material is available free of charge via the Internet at http://pubs.acs.org.

■ AUTHOR INFORMATION

Corresponding Author

*Tel: +1 541 737 5808. Fax: +1 541 737 3999. E-mail: kerry.mcphail@oregonstate.edu

Notes

The authors declare no competing financial interest.

■ ACKNOWLEDGMENTS

We thank Professor Bill Fenical of Scripps Institution of Oceanography, San Diego, CA for the generous donation of funding which enabled the first large scale SCUBA collection of marine ascidians in Algoa Bay, South Africa. We are also grateful to Rodger Kohnert for NMR technical assistance, and Brian Arbogast and Jeff Morre of the Environmental Health Sciences Center at OSU for mass spectrometric data acquisition (NIEHS P30 ES00210). The National Science Foundation (CHE-0722319) and the Murdock Charitable Trust (2005265) are acknowledged for their support of the OSU Natural Products and Small Molecule Nuclear Magnetic Resonance. Additional funding was provided by the OSU College of Pharmacy.

■ REFERENCES

(1) Blunt, J. W.; Copp, B. R.; Keyzers, R. A.; Munro, M. H. G.; Prinsep, M. R. *Nat. Prod. Rep.* **2012**, *29*, 144.
(2) Molinski, T. F.; Dalisay, D. S.; Lievens, S. L.; Saludes, J. P. *Nat. Rev. Drug Discovery* **2009**, *8*, 69.
(3) Ueda, K.; Hu, Y. *Tetrahedron Lett.* **1999**, *40*, 6305.
(4) Corley, D. G.; Moore, R. E.; Paul, V. J. *J. Am. Chem. Soc.* **1988**, *110*, 7920.

(5) Zabriskie, T. M.; Mayne, C. L.; Ireland, C. M. *J. Am. Chem. Soc.* **1988**, *110*, 7919.
(6) Schupp, P.; Poehner, T.; Edrada, R.; Ebel, R.; Berg, A.; Wray, V.; Proksch, P. *J. Nat. Prod.* **2002**, *66*, 272.
(7) Fu, X.; Palomar, A. J.; Hong, E. P.; Schmitz, F. J.; Valeriote, F. A. *J. Nat. Prod.* **2004**, *67*, 1415.
(8) Tsukimoto, M.; Nagaoka, M.; Shishido, Y.; Fujimoto, J.; Nishisaka, F.; Matsumoto, S.; Harunari, E.; Imada, C.; Matsuzaki, T. *J. Nat. Prod.* **2011**, *74*, 2329.
(9) Schmidt, E. W.; Sudek, S.; Haygood, M. G. *J. Nat. Prod.* **2004**, *67*, 1341.
(10) Ogi, T.; Margiastuti, P.; Teruya, T.; Taira, J.; Suenaga, K.; Ueda, K. *Mar. Drugs* **2009**, *7*, 816.
(11) Schmidt, E. W.; Donia, M. S.; McIntosh, J. A.; Fricke, W. F.; Ravel, J. *J. Nat. Prod.* **2012**, *75*, 295.
(12) Xu, Y.; Kersten, R. D.; Nam, S.-J.; Lu, L.; Al-Suwailem, A. M.; Zheng, H.; Fenical, W.; Dorrestein, P. C.; Moore, B. S.; Qian, P.-Y. *J. Am. Chem. Soc.* **2012**, *134* (20), 8625−8632.
(13) Cicero, D. O.; Barbato, G.; Bazzo, R. *J. Magn. Reson.* **2001**, *148*, 209.
(14) Tanaka, J.-i.; Higa, T. *Tetrahedron Lett.* **1996**, *37*, 5535.
(15) Grindley, T. B. In *Glycoscience: Chemistry and Chemical Biology*, 2nd ed.; Fraser-Reid, B. O., Tatsuta, K., Thiem, J., Coté, G. L., Flitsch, S., Ito, Y., Kondo, H., Nishimura, S.-i., Yu, B., Eds.; Springer-Verlag: Germany, 2008; Vol. *1*, p 11.
(16) Gheysen, K.; Mihai, C.; Conrath, K.; Martins, J. C. *Chem.−Eur. J* **2008**, *14*, 8869.
(17) Bock, K.; Pedersen, C. *J. Chem. Soc., Perkin Trans. 2* **1974**, 293.
(18) Motohashi, K.; Takagi, M.; Shin-ya, K. *J. Nat. Prod.* **2010**, *73*, 755.
(19) Seo, S.; Tomita, Y.; Tori, K.; Yoshimura, Y. *J. Am. Chem. Soc.* **1978**, *100*, 3331.
(20) Chini, M. G.; Jones, C. R.; Zampella, A.; D'Auria, M. V.; Renga, B.; Fiorucci, S.; Butts, C. P.; Bifulco, G. *J. Org. Chem.* **2012**, *77*, 1489.
(21) Winder, P. L. Ph.D. Thesis, Florida Atlantic University, 2009.
(22) Thornburg, C. C.; Thimmaiah, M.; Shaala, L. A.; Hau, A. M.; Malmo, J. M.; Ishmael, J. E.; Youssef, D. T. A.; McPhail, K. L. *J. Nat. Prod.* **2011**, *74*, 1677.
(23) Uhrín, D.; Batta, G.; Hruby, V. J.; Barlow, P. N.; Kövér, K. E. *J. Magn. Reson.* **1998**, *130*, 155.
(24) Sugahara, K.; Kitamura, Y.; Murata, M.; Satake, M.; Tachibana, K. *J. Org. Chem.* **2011**, *76*, 3131.
(25) Navarro-Vázquez, A.; Cobas, J. C.; Sardina, F. J.; Casanueva, J.; Díez, E. *J. Chem. Inf. Comput. Sci.* **2004**, *44*, 1680.
(26) Parish, C.; Lombardi, R.; Sinclair, K.; Smith, E.; Goldberg, A.; Rappleye, M.; Dure, M. *J. Mol. Graphics Modell.* **2002**, *21*, 129.
(27) Foloppe, N.; Chen, I.-J. *Curr. Med. Chem.* **2009**, *16*, 3381.
(28) Lu, Z.; Van Wagoner, R. M.; Harper, M. K.; Baker, H. L.; Hooper, J. N. A.; Bewley, C. A.; Ireland, C. M. *J. Nat. Prod.* **2011**, *74*, 185.
(29) Evtushenko, E. V. *Carbohydr. Res.* **1999**, *316*, 187.